



Li₂SiO₃ fast microwave-assisted hydrothermal synthesis and evaluation of its water vapor and CO₂ absorption properties



J. Ortiz-Landeros^{a,*}, R. López-Juárez^b, I.C. Romero-Ibarra^c, H. Pfeiffer^d,
H. Balmori-Ramírez^a, C. Gómez-Yáñez^a

^a Department of Metallurgical and Materials Engineering, National Polytechnic Institute, ESIQJE-IPN, UPALM Campus, Instituto Politécnico Nacional Avenue, 07738 Mexico City, Mexico

^b Materials Research Institute Morelia Campus, National Autonomous University of Mexico, Old Pátzcuaro road 8701, 58190 Morelia, Michoacán, Mexico

^c Department of Chemistry, Metropolitan Autonomous University, Iztapalapa Campus, San Rafael Atlixco Avenue 186, 09340 Mexico City, Mexico

^d Materials Research Institute, National Autonomous University of Mexico, Cd Universitaria Campus, 04510 Mexico City, Mexico

ARTICLE INFO

Article history:

Received 7 January 2015

Received in revised form 16 March 2015

Accepted 21 March 2015

Available online 21 August 2015

Keywords:

CO₂ capture

Lithium metasilicate

Hydrothermal synthesis

Thermal analysis

ABSTRACT

A series of lithium metasilicate (Li₂SiO₃) powder materials has been successfully synthesized by the microwave-assisted hydrothermal route using lithium hydroxide and tetraethyl-orthosilicate-derived sol precursors. Ceramic powders were obtained under hydrothermal conditions of autogenous pressure in the presence of a nonionic surfactant. The production of pure and well-crystallized Li₂SiO₃ using very short reaction times at low temperatures was shown by X-ray diffraction, scanning electron microscopy, and N₂ adsorption-desorption analyses. Synthesized Li₂SiO₃ particles were nanocrystalline and exhibited different morphologies and specific surface areas depending on the synthesis conditions. Additionally, the capability of selected Li₂SiO₃ samples to absorb H₂O and CO₂ was evaluated via thermogravimetric analyses by varying the temperature, carrier gas, and water vapor concentration. Li₂SiO₃ particles exhibited interesting textural and morphological characteristics that make them suitable for use as a CO₂ absorbent and which suggest that they also have the potential to be used in other applications.

© 2015 Chinese Society of Particuology and Institute of Process Engineering, Chinese Academy of Sciences. Published by Elsevier B.V. All rights reserved.

Introduction

In recent years, lithium ceramics have been studied primarily because of their technological applications in the design of breeder ceramics for the nuclear industry (Carella & Hernández, 2012; Knitter, Chaudhuri, Feng, Hoshino, & Yu, 2013a; Knitter, Kolb, Kaufmann, & Goraieb, 2013b), as well as their promise as ionic conductor materials in the fabrication of Li-ion batteries (Peng et al., 2009; Inaguma & Nakashima, 2013; Tatsumisago, Takano, Tadanaga, & Hayashi, 2014). Other potential applications include the preparation of heterogeneous catalysts (Wang et al., 2012; Puna, Gomes, Bordado, Correia, & Dias, 2014), ceramic membranes (Nair, Burwood, Goh, Nakagawa, & Yamaguchi, 2009; Nomura, Sakanishi, Utsumi, & Nakamura, 2013), and solid sorbents for CO₂ capture in post-combustion processes (Ortiz-Landeros, Romero-Ibarra, Gómez-Yáñez, Lima, & Pfeiffer, 2013; Yang, 2010).

In the last case, lithium-containing sorbents are able to selectively trap CO₂ across a wide range of temperatures and CO₂ concentrations (Wang et al., 2014). Among lithium ceramics, lithium metasilicate (Li₂SiO₃) is of research interest in several fields of study.

Pure Li₂SiO₃ can be synthesized by solid-state reaction (Prasad & Basu, 2012; Tang, Zhang, Meng, & Luo, 2009). However, this method offers a limited control of the final microstructure. For instance, it is difficult to obtain nanocrystalline particles of Li₂SiO₃ via the conventional ceramic method, as the firing of raw materials at relatively elevated temperatures (700–1000 °C) promotes sintering and, eventually, crystal growth (Cruz, Bulbulian, Lima, & Pfeiffer, 2006; Tang et al., 2009). In this sense, the remarkable differences in the microstructures of lithium silicate powders prepared by other non-conventional methods could be a key factor in improving the performance of this material for specific applications. For instance, it has been noted that the porosity and particle size of lithium ceramics are closely related to the tritium release rate and reactivity in ceramic breeders and CO₂ ceramic sorbents, respectively (Carella & Hernández, 2012; Romero-Ibarra, Ortiz-Landeros, & Pfeiffer, 2013; Slagle, Hollenberg, & Baldwin, 1991).

* Corresponding author. Tel.: +52 5557296000x54267;
fax: +52 5557296000x54267.

E-mail address: jortiz@ipn.mx (J. Ortiz-Landeros).

Therefore, from the point of view that the preparation of Li_2SiO_3 is a critical step to obtain useful materials for advanced applications, emerging synthetic approaches have to be taken into account. Until now, some chemical routes have been explored to synthesize Li_2SiO_3 powders, such as sol-gel (Li et al., 2011; Zhang, Nieuwoudt, & Easteal, 2008), microemulsion (Khomane, Sharma, Saha, & Kulkarni, 2006), combustion (Cruz & Bulbulian, 2003; Mondragón-Gutiérrez, Cruz, Pfeiffer, & Bulbulian, 2008), mechanosynthesis (Yang, Wang, Li, & Shi, 2012), and hydrothermal techniques (Alemi, Khademinia, Joo, Dolatyari, & Bakhtiari, 2013; Ortiz-Landeros, Contreras-García, Gómez-Yáñez, & Pfeiffer, 2011b). Hydrothermal synthesis offers several advantages, including the production of crystalline powders at low temperature, the control of particle size and shape, the production of soft aggregates (or even a lack of aggregates), and a homogeneous composition and stoichiometry of the phases (Li & Yang, 2014; Ortiz-Landeros, Gómez-Yáñez, López-Juárez, Dávalos-Velasco, & Pfeiffer, 2012; Somiya & Roy, 2000). Moreover, it is assumed that the use of microwave heating during hydrothermal synthesis could offer certain additional benefits, including the fast dissolution of precursors, a significant reduction of reaction times, and volumetric heating that enhances the preparation of ultrafine and monodisperse powders (Ortiz-Landeros et al., 2012).

Based on the above, the aim of this work was to study Li_2SiO_3 synthesis by the microwave-assisted hydrothermal approach and to establish the effect of the synthetic route on the resultant Li_2SiO_3 properties. This chemical route was chosen to obtain particulate materials with novel structural and microstructural characteristics that could promote their performance for emerging applications, such as CO_2 absorbents and solid basic catalysts, among others.

Experimental

Preparation of Li_2SiO_3 powders

$\text{LiOH}\cdot\text{H}_2\text{O}$ (90%, Sigma-Aldrich, MO, USA) reagent was dissolved in an aqueous ethanol solution (30:70 EtOH: H_2O). Then, a stoichiometric amount of tetraethyl orthosilicate (TEOS, Si-(OC_2H_5)₄, Sigma-Aldrich) required to obtain a 2:1 molar ratio of Li:Si was added dropwise to the solution. The precursor solution was subsequently stirred using an ultrasonic bath for 15 min to obtain a gel that was transferred into a MARS 6 reactor (CEM, NC, USA) for the microwave-assisted hydrothermal treatment of lithium metasilicate. The apparatus is equipped with a series of stirred and hermetically sealed Teflon reaction vessels and a microwave heating system. The oven power source was fixed at 800 W. Pressurized reactions were performed for 15 and 30 min under autogenous conditions that reached 125 °C. After the hydrothermal reaction, samples were washed and dried. Other variables studied were the use of mechanical stirring during the hydrothermal process and the addition of surfactant. In the latter case, the surfactant was octylphenol ethylene oxide condensate (Triton X-114). This non-ionic surfactant was used in an amount equivalent to 25 times the critical micelle concentration at 25 °C ($\text{CMC} = 0.205 \times 10^{-3}$ mol/L).

A reference sample of lithium metasilicate was synthesized by the conventional solid-state reaction method using silicic acid (H_2SiO_3 , Avantor Performance Materials, PA, USA) and lithium carbonate (Li_2CO_3 , Sigma-Aldrich) as starting reactants. The powder mixture was prepared at a stoichiometric Li:Si molar ratio of 2:1 and heat-treated at 900 °C for 6 h in air.

The different samples, i.e., those synthesized via solid-state reaction, via microwave-assisted hydrothermal synthesis, microwave-assisted hydrothermal synthesis with mechanical stirring, or via the addition of surfactant, were labeled as SSR, MH, MH-Stirring, MH-Surfactant, respectively.

Characterization of Li_2SiO_3 powders

Structural and microstructural characterization was carried out by powder X-ray diffraction (XRD), scanning electron microscopy (SEM) and N_2 adsorption techniques. XRD patterns of the differently prepared samples were recorded on a Bruker (MA, USA) AXS diffractometer model D8-Advance equipped with a Cu anode X-ray tube in the Bragg-Brentano configuration and a Ge monochromator. Additionally, for crystalline phase identification, Rietveld structural refinements were conducted by following the full pattern fitting method using FullProf-Suite software (Roisnel & Rodriguez-Carvajal, 2000). The profile function, which was used to describe the peak shape, was a pseudo-Voigt function. The instrumental profile was determined by the Caglioti function, where the parameters u , v , and w were refined according to the LaB_6 standard sample.

The scanning electron microscopy (SEM) analysis was performed using a JEOL JSM-6400 microscope (MA, USA).

Characterization of the specific surface area (SSA) and porosity features of the Li_2SiO_3 powders was carried out by N_2 sorption measurements using a BELsorp-mini II analyzer (BEL Japan, Osaka, Japan). The samples were degassed at 90 °C under vacuum for 12 h. SSA_{BET} values were obtained from the N_2 adsorption isotherms using the Brunauer, Emmett and Teller (BET) model. The pore volume was calculated on the basis of the amount of adsorbed N_2 after completing pore condensation at a relative pressure of $P/P_0 = 0.995$. The pore size distribution was determined by the Barrett, Joyner, and Halenda (BJH) method.

H_2O and CO_2 absorption evaluation

Selected samples were subjected to different water vapor and CO_2 absorption tests. First, the water vapor absorption capacity of the prepared materials was evaluated by thermogravimetric analysis using a gravimetric vapor sorption analyzer (Q5000SA, TA Instruments, USA). The water capture tests were performed at 30 and 50 °C and at relative humidities (RHs) ranging from 0 to 80% under a 100% N_2 (high purity grade, 99.99% INFRA, Mexico) atmosphere and from 30 °C to the target temperature at a temperature-heating rate of 1.0 °C/min.

Then, to evaluate the CO_2 absorption capacity, a thermogravimetric analysis of Li_2SiO_3 carbonation in the presence of water vapor was conducted under the same experimental conditions described above, but sorption tests were performed using 100% CO_2 (research grade, 99.8% INFRA) as the carrier gas.

Additionally, different CO_2 absorption curves were obtained by thermogravimetric isothermal analyses at 20, 40, 60, and 80 °C at RHs ranging from 20% to 80%. Once the system reached the desired humidity values, the change in mass due to carbonation was monitored for 180 min.

Finally, after the water absorption and carbonation tests, the reaction products were analyzed using a Nicolet 6700 Fourier transform-infrared spectrometer (FT-IR, Thermo Fisher Scientific, USA).

Results and discussion

Structural and microstructural characterization of Li_2SiO_3 powders

Fig. 1 shows the recorded XRD patterns, in which the Li_2SiO_3 phase was identified in all of the samples according to the JCPDS card No. 00-029-0828. However, certain differences were observed in the diffraction profiles. First, the solid-state reaction sample (Fig. 1(a)) had an impurity of lithium orthosilicate phase (Li_4SiO_4 , JCPDS card No. 00-076-1085). As it is well known, the occurrence of

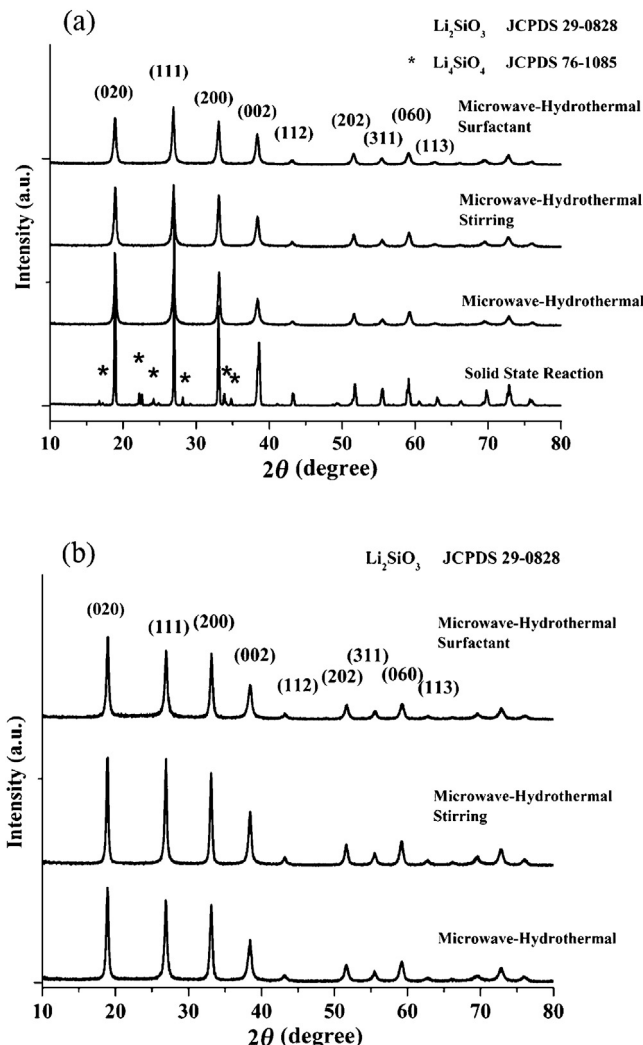


Fig. 1. XRD patterns of the Li_2SiO_3 samples obtained under different synthesis conditions: (a) SSR sample and a series of samples obtained via 15-min hydrothermal reaction and (b) a series of samples obtained via 30-min hydrothermal reaction.

segregated components or secondary phases is a common issue in the synthesis of ceramic oxides via conventional ceramic methods. In contrast, the hydrothermally synthesized samples only exhibited the pure Li_2SiO_3 phase. Additionally, it is outstanding that the mild synthesis conditions used, 15- or 30-min hydrothermal reaction times at a low temperature of 125°C , yielded well-crystallized Li_2SiO_3 . These series of samples showed broader diffraction peaks that suggest that the small crystallite size was the result of the synthesis method.

For the sake of brevity, further characterization was only conducted on the materials obtained using the 15-min reaction time. First, an XRD refinement analysis was conducted. All of the samples fitted reasonably well to the Rietveld analyses. Fig. 2 shows an example of the refined diffraction pattern. The obtained R_{wp} values were less than 10% in all of the cases, supporting that the refinements were acceptable. The inset in Fig. 2 shows the modeled Li_2SiO_3 crystal structure. The cell parameters and the crystallite sizes obtained in each case are presented in Table 1. The cell parameters did not differ significantly between the synthesis conditions. In contrast, the crystallite sizes showed remarkable differences depending on the synthesis conditions. Meanwhile, the SSR sample had an average crystallite size of 348 nm, the MH sample exhibited

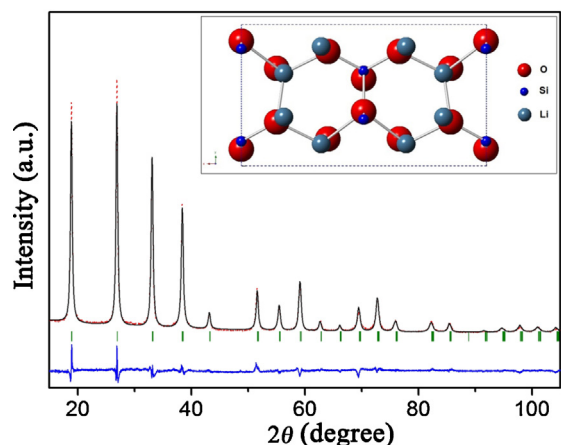


Fig. 2. Rietveld refined XRD pattern for hydrothermally synthesized Li_2SiO_3 . The difference between the experimental pattern (red solid line) and calculated data (blue dashed line) is shown at the bottom of the panel (blue solid line). The calculated reflection locations are indicated by vertical markers. (For interpretation of the references to color in this figure legend, the reader is referred to the web version of this article.)

Table 1
Rietveld refinement data obtained from the different Li_2SiO_3 samples.

Sample	Crystallite size (nm)	Cell parameters (\AA)		
		a	b	c
Ref	—	9.396	5.396	4.661
SSR	348	9.398	5.397	4.659
MH	27	9.319	5.389	4.664
MH-Stirring	22	9.354	5.401	4.669
MH-Surfactant	17	9.349	5.383	4.666

a crystallite size of 27 nm. This is because volumetric heating mitigates thermal gradients, which favors homogeneous nucleation and growth processes during the hydrothermal reaction (Ortiz-Landeros et al., 2012). Additionally, the stirring seems to have an effect on the crystallite size, as it was slightly reduced to 22 nm. The observed effect of stirring is in agreement with the results reported by Komarneni and Katsuki (2010), who concluded that stirring led to smaller and more uniform crystals of barium titanate ceramic powders under microwave hydrothermal conditions compared with those that were crystallized without stirring.

Moreover, the smallest crystallite size of 17 nm was obtained using a surfactant during the hydrothermal synthesis (Table 1). It is believed that the surfactant molecules are adsorbed onto the surface of the formed primary particles, and the presence of these molecules hinders the aggregation and further coalescence of the ceramic particles (Ortiz-Landeros et al., 2011b).

SEM images (Fig. 3) show the morphology of the final particles and aggregates constituting the various samples. The SSR sample consists of micrometric and dense particles in the range of 2–8 μm , which form aggregates of about 50–150 μm . In contrast, as was expected, the particle size of the hydrothermally synthesized samples was much smaller than that of the sample prepared by SSR. In general, Li_2SiO_3 powder comprises micrometric and spheroidal-like aggregates that are composed of nanometric particles. Additionally, a careful observation reveals that the powder is made of hollow aggregates, with individual nanoparticles forming porous walls (inset Fig. 3(b)–(d)). The microstructural details of samples obtained at various reaction conditions are shown in the images of the broken spheres (inset of Fig. 3(b)–(d)). An interesting feature is that the use of a surfactant promotes the formation of smaller spherical aggregates of approximately 380–420 nm, which, in fact, form the walls of larger micrometric

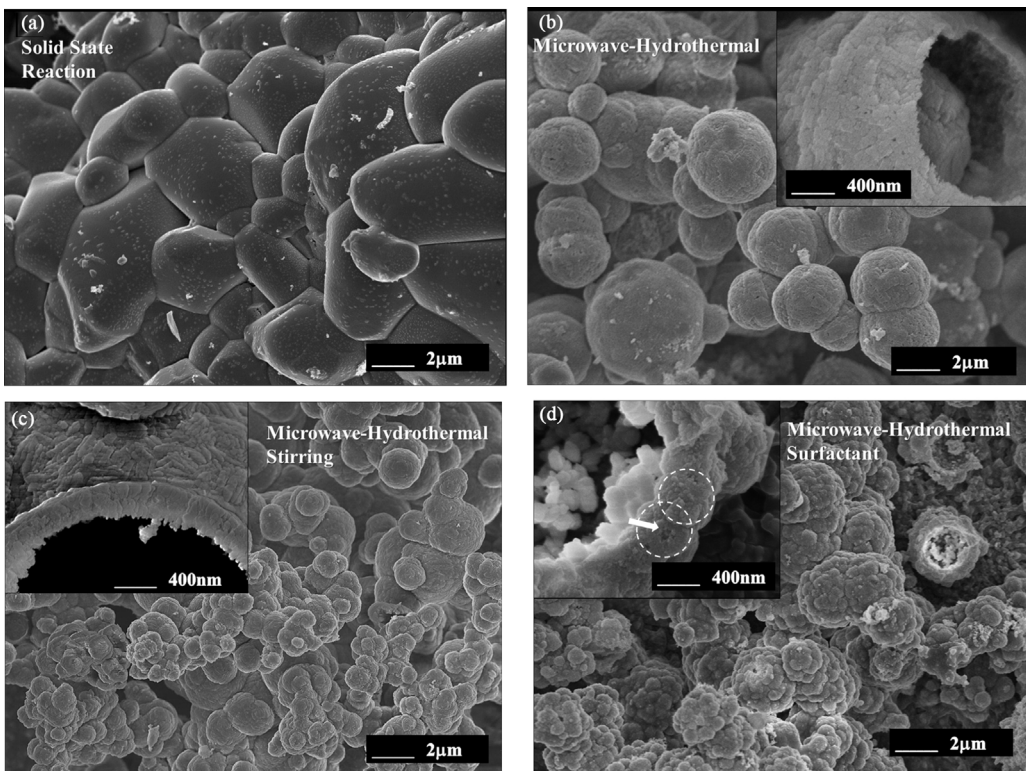


Fig. 3. SEM images of the different Li_2SiO_3 powders.

aggregates (inset Fig. 3(d)). These morphologies are the result of the formation of supramolecular arrays of surfactant molecules that act as soft templates during the hydrothermal process. Based on the size of these aggregates, it is believed that the aforesaid surfactant arrays are vesicles (Ortiz-Landeros et al., 2011b).

Fig. 4 shows the N_2 adsorption-desorption isotherms of different Li_2SiO_3 samples synthesized in 15 min. According to classical IUPAC classification, the SSR sample presented a type III isotherm (Fig. 4(a)). This is based on the fact that it has no clear B point. Additionally, in this case, the C value (Table 2) is the smallest of the series, suggesting that there was a weaker adsorbent–adsorbate interaction than in the other samples.

In contrast, according to the IUPAC extended classification reported by Rouquerol, Rouquerol, and Sing (1999), all the hydrothermally synthesized samples presented type IIb isotherms. This isotherm is associated with a monolayer–multilayer adsorption on an open, external surface of a non-porous or macroporous solid (Leofanti, Padovan, Tozzola, & Venturelli, 1998; Rouquerol et al., 1999). In contrast to the SSR powder, the MH, MH-Stirring, and MH-Surfactant samples exhibited significant hysteresis with an H3 type loop (Fig. 4(b)). Type IIb isotherms are characteristic of many aggregated powders that possess inter-particle, slit-shaped pores. In certain cases, these types of pores have a non-rigid constitution, such as clay aggregates and some pigments (Rouquerol et al., 1999). Type IIb isotherms show capillary condensation and hysteresis, but in contrast to the classical type IV isotherm, there is no plateau at high P/P_0 . In the present work, these characteristic physisorption behaviors can be attributed to the formation of porous aggregates, such as those commonly obtained by hydrothermal methods (Li & Yang, 2014; Ortiz-Landeros et al., 2012; Somiya & Roy, 2000).

As was expected, all the ceramics that were hydrothermally synthesized had larger surface areas than that of the SSR sample (Table 2). Considering the type of isotherm, the selected range of linearity to apply the BET model was $0.075 < P/P_0 < 0.15$.

Additionally, the C values ranged from 72.1 to 128.9, which is consistent with nitrogen adsorption at the monolayer condition (Rouquerol et al., 1999). The lowest and highest surface areas, 0.2 and $37.3 \text{ m}^2/\text{g}$, correspond to the SSR and MH-Surfactant samples, respectively. This result is in agreement with the microstructural features observed by SEM, which showed the presence of porous aggregates in the case of the MH-Surfactant sample.

Moreover, Fig. 5 shows the estimated pore size distributions of the different samples for comparative purposes. Synthesized powders exhibited mesoporosity, with pore sizes between 8.3 and 9.7 nm. The largest pore volumes were obtained for the MH-Surfactant sample. These textural characteristics are important both for sorption and the catalysts' applications, as they promote fast mass transport.

Water vapor absorption

The effect of microstructure (crystallite size, particle size, porosity, and SSA) on the water sorption and carbonation processes was studied. For comparison purposes, the SSR and MH-Surfactant samples were analyzed. In the first step, water vapor sorption was conducted under different humidities and temperatures. Fig. 6(a) shows the isotherm of the MH-Surfactant sample under a pure N_2 atmosphere. For the MH-Surfactant sample, the observed weight increments were very small (<1.6 wt%), and the isotherms showed a similar behavior during sorption and desorption at 50°C . Actually, after desorption, the samples did not register a final weight gain. Therefore, these results suggest that under these experimental conditions, the samples only experienced an incipient physisorption process that occurred because of the condensation of water vapor at high RHs (40–80%); then, during desorption, when the RH was less than 40%, the trapped water was completely desorbed (Fig. 6(a)).

Fig. 6(b) shows the corresponding FT-IR spectra. The data confirm the negligible reaction of samples under low temperatures and humidities. The bands at approximately 615 , 736 , and 980 cm^{-1} are

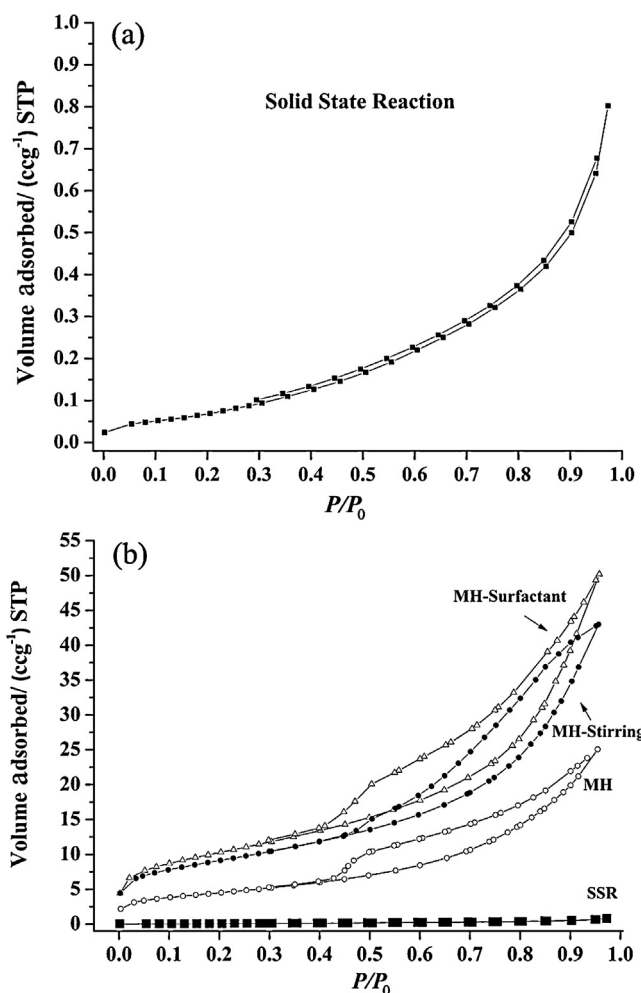


Fig. 4. N₂ physisorption isotherms of different Li₂SiO₃ powders: (a) SSR and (b) SSR and hydrothermally synthesized samples.

attributed to the different vibration modes of the Si—O—Si bond of the silicate (Zhang et al., 2008). The band at 938 cm⁻¹ is due to the vibration of the O—Si—O bond. The bands located at 490 and 856 cm⁻¹ are attributed to the terminal bonds Si—O⁻ and O—Si—O⁻, respectively (Li & Yang, 2014; Yang et al., 2012; Zhang et al., 2008). A small band located at 1438 cm⁻¹ corresponds to the lithium carbonate; this compound also showed a band at 856 cm⁻¹, which must have overlapped with the vibration of the O—Si—O⁻ bond. The band at 1050 cm⁻¹ is due to the Si—O—Si bond of the silica (Ortiz-Landeros et al., 2011b; Zhang et al., 2008). As these absorption tests did not involve the use of CO₂ gas, but involved N₂ instead, the presence of carbonate must be due to the incipient surface carbonation of materials during storage and handling in the CO₂ containing atmosphere. Bands due to the vibration of O—H bonds in water molecules were not observed. Based on its textural and

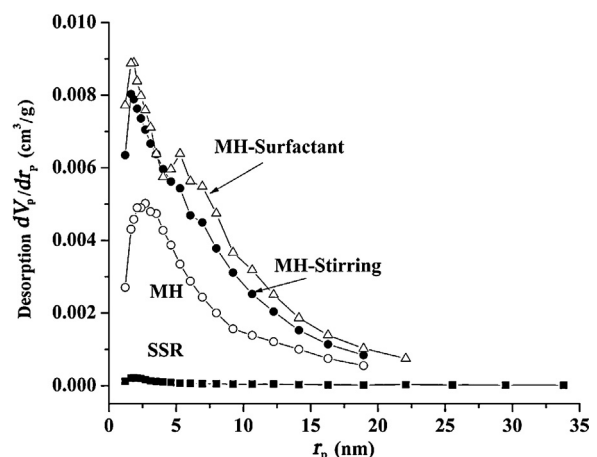


Fig. 5. Estimated pore size distribution of the differently synthesized Li₂SiO₃ samples.

morphological characteristics (Section 3.1), as well as the fact that Li₂SiO₃ does not show a significant reactivity with water, these results suggest the potential application of these materials in the fabrication of stable, heterogeneous catalysts for the production of biodiesel (Chen et al., 2013; Wang, Chen, Huang, & Chen, 2011).

Carbonation of Li₂SiO₃ in the presence of water vapor

Regarding the Li₂SiO₃ carbonation behavior, absorption experiments were conducted under different water vapor concentrations (0–80% RH) at different temperatures; in this case, pure CO₂ was used as the carrier gas. Fig. 7(a) shows the CO₂—H₂O_(v) sorption isotherms of MH-Surfactant samples at 30, 50, and 70 °C. The results show a clear enhancement of sorption with increasing temperature. Additionally, Fig. 7(b) shows the CO₂—H₂O_(v) sorption isotherms of the different samples that were generated as a function of the RH. The isotherms show a very small weight increment of approximately 0.49 wt% for the SSR sample at 50 °C. In contrast, the MH, MH-Stirring, and MH-Surfactant samples exhibited significant weight increments of 7.8, 13.9, and 20.6 wt%, respectively, at 50 °C.

Despite the fact that thermodynamic calculations suggest that Li₂SiO₃ is able to react with CO₂ to form lithium carbonate under dry conditions and low temperatures, ranging from room temperature to about 250 °C (Reaction (a)), the observed reaction kinetics are very slow. Actually, the carbonation of the materials was only observed by thermogravimetric analysis under humid conditions. It is believed that carbonation in the presence of water vapor (Reaction (b)) takes place through the formation of more reactive intermediate species, such as LiOH (Reaction (c)), which are formed on inactive sites of the solid surface, such as terminal bonds and, perhaps, enriched lithium zones (Ortiz-Landeros, Gómez-Yáñez, & Pfeiffer, 2011c). Additionally, theoretical thermodynamic data calculated by FACTSage (Equilib-module) thermochemical software

Table 2
Textural properties of the different Li₂SiO₃ powders.

Sample	Textural properties			
	SSA _{BET} (m ² /g)	Mean pore diameter ^a (nm)	Total pore volume ^b (cm ³ /g)	C (0.075 < P/P ₀ < 0.15)
SSR	0.2	—	—	72.1
MH	16.2	9.7	0.04	108.8
MH-Stirring	32.8	8.3	0.66	128.9
MH-Surfactant	37.3	8.5	0.87	99.4

^a Calculated based on desorption isotherms and the BJH model.

^b Calculated based on N₂ adsorption and P/P₀ = 0.975.

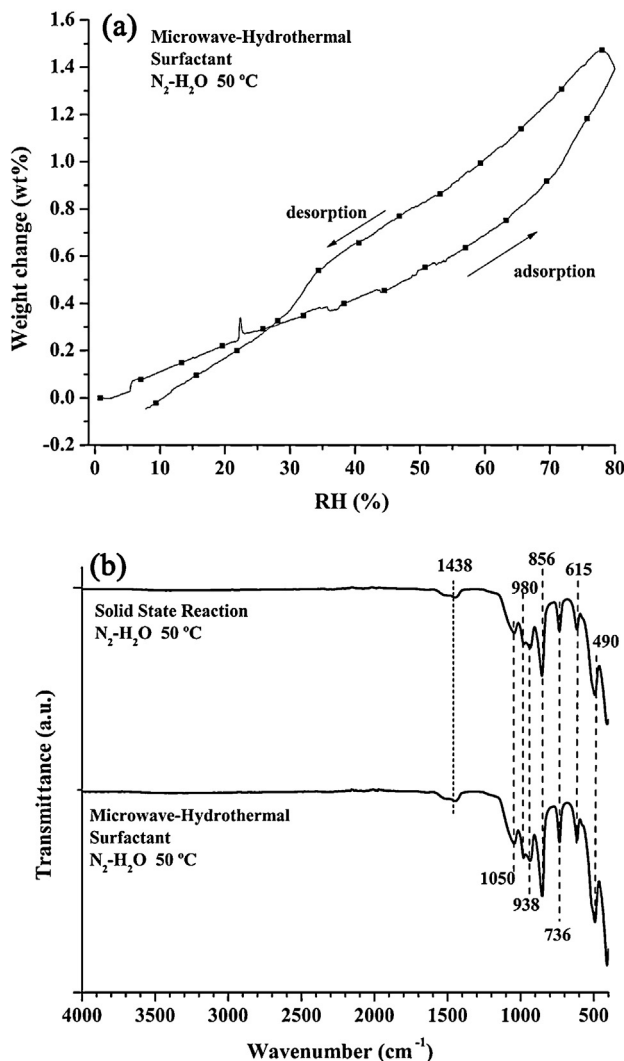
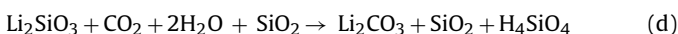
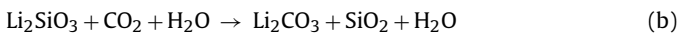
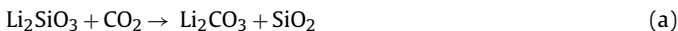


Fig. 6. Isotherms of water adsorption at different relative humidities under N_2 flow: (a) water vapor sorption isotherms and (b) FT-IR spectra of the materials after desorption.

(Bale et al., 2002) suggest the occurrence of other minority equilibrium species, such as carbonic acid and silicic acid, which are formed by the dissolution of silica via a hydration reaction (Reaction (d)).



To corroborate the Li_2SiO_3 carbonation and, therefore, the consequent formation of Li_2CO_3 , SiO_2 , and H_4SiO_4 species according to reactions (b) and (d), the SSR and MH-Surfactant samples were analyzed by FT-IR and XRD after the $\text{CO}_2\text{-H}_2\text{O}_{(\text{v})}$ chemisorption test at 50 °C. Fig. 8 shows the corresponding FT-IR spectra. The data confirm the carbonation of the samples. Similar to the previous results, the bands at approximately 612, 734, and 980 cm^{-1} are attributed to the different vibration modes of the Si—O—Si bond of the silicate (Zhang et al., 2008). The band at 936 cm^{-1} is due to the vibration of the O—Si—O bond. The bands located at 490 and 852 cm^{-1} are due to the terminal bonds Si—O⁻ and O—Si—O⁻, respectively. The bands at 1436 and 852 cm^{-1} correspond to the Li_2CO_3 . Finally, the band at 1052 cm^{-1} is due to the Si—O—Si bond of the SiO_2 . It can be observed

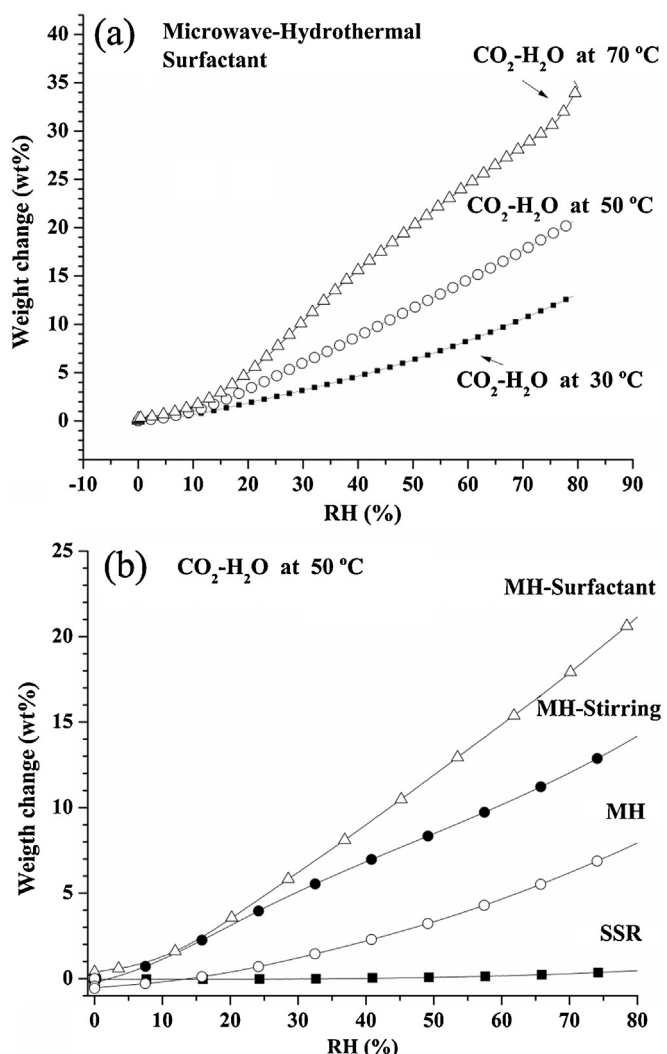


Fig. 7. Isotherms of water absorption at different relative humidities under CO_2 flow: (a) MH-Surfactant sample at 30, 50 and 70 °C and (b) absorption isotherms of the different synthesized samples at 50 °C.

that the bands corresponding to the Li_2CO_3 and SiO_2 bonds are much higher in intensity in the MH-Surfactant sample than in the SSR sample because of the different degree of carbonation according to reaction (b). The presence of other minority species, such as silicic acid, was not observed, in part because the bands of the Si—O and Si—O—H bonds of silicic acid would be located at 939 and 1042–1090 cm^{-1} (Swedlund, Miskelly, & McQuillan, 2009), and, therefore, these signals would overlap with the silica bands in the obtained FT-IR spectra. However, taking into account that the formation of silicic acid was negligible, in the subsequent CO_2 capture analysis, it was considered that carbonation takes place according to reaction (b), or, in other words, that water chemisorption does not occur. It is also important to emphasize that the FT-IR spectra of the reaction products did not reveal the presence of water molecules; therefore, based on these results, it can be assumed that the observed final mass gains are not due to the condensation of physisorbed water, but solely due to carbonation. These results are in agreement with those of previous reports (Ortiz-Landeros et al., 2011b; Ortiz-Landeros, Martínez-dlCruz, Gómez-Yáñez, & Pfeiffer, 2011a).

Fig. 9 shows the XRD patterns of the MH-Surfactant sample before and after the $\text{CO}_2\text{-H}_2\text{O}_{(\text{v})}$ chemisorption test at 50 °C. All of the observed diffraction peaks were identified in accordance with

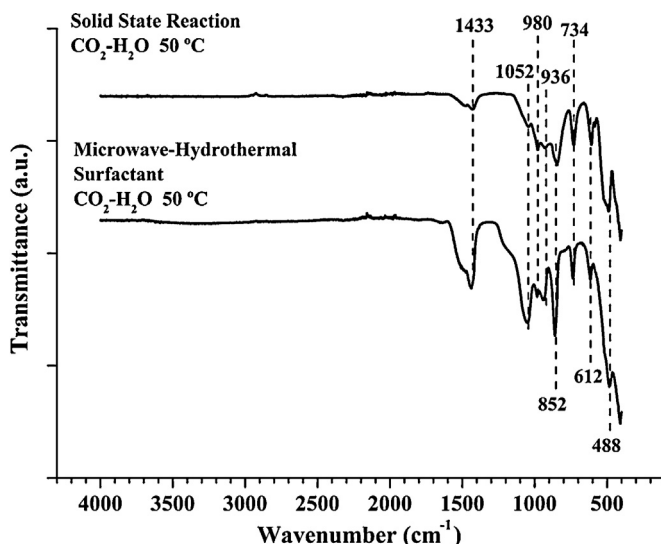


Fig. 8. FT-IR spectra of the Li_2SiO_3 powders after $\text{CO}_2\text{-H}_2\text{O}(\nu)$ chemisorption.

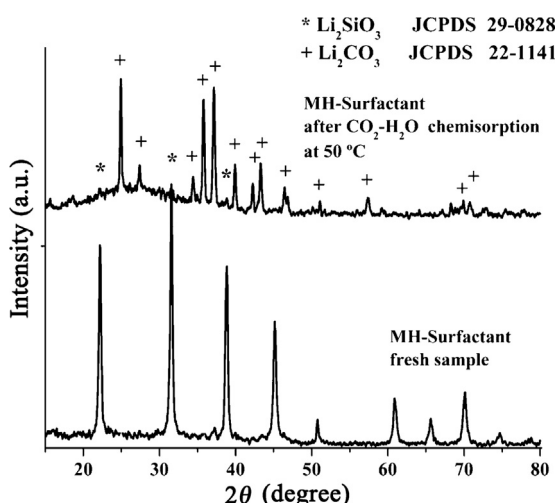


Fig. 9. XRD patterns of the Li_2SiO_3 powder before and after the $\text{CO}_2\text{-H}_2\text{O}(\nu)$ chemisorption test at 50°C .

the JCPDS database. After carbonation, the sample was composed of the lithium carbonate (Li_2CO_3) crystalline phase. Because the reaction was not completed under these experimental conditions, the reflections of the remaining Li_2SiO_3 phase were also identified. Additionally, the presence of the SiO_2 as an amorphous phase was demonstrated because of the broad signal observed from 20° to 35° in 2θ . The XRD analysis agrees with the FT-IR results and confirms that carbonation reactions take place according to reaction (b).

Kinetic analysis of Li_2SiO_3 carbonation

Several kinetic models have been applied to describe the carbonation process of ceramic materials in the presence of water vapor (Nikulshina, Gálvez, & Steinfeld, 2007; Nikulshina & Steinfeld, 2009; Shih, Ho, Song, & Lin, 1999; Siauciunas, Rupsyté, Kitrys, & Galeckas, 2004). In the present work, the kinetic model proposed by Shih et al. (1999) was used to study the carbonation of Li_2SiO_3 . This model has been successfully used to study the carbonation of $\text{Ca}(\text{OH})_2$ in the presence of water vapor. Briefly, the model assumes that carbonation is controlled by surface reaction, and that surface reaction occurs on a reactive surface that is not covered by the

formed products. The relationship between conversion and time is as follows:

$$X = \frac{[1 - \exp(-K_1 K_2 t)]}{K_2}, \quad (1)$$

where K_1 and K_2 are defined as

$$K_1 = K_s S_g M, \quad (2)$$

$$K_2 = \frac{K_p}{(S_g M)}, \quad (3)$$

where K_s and K_p are functions of the temperature, the concentrations of reacting species, and RH. S_g and M are the initial specific surface area of the solid and its molecular weight, respectively. Based on the above, K_1 and K_2 would be functions of the SSA of the solid, temperature, CO_2 concentration, and RH. However, in the present study, it can be assumed that K_1 and K_2 are independent of the CO_2 concentration, because a constant flow of pure CO_2 was used as the carrier gas in the experiments. The Li_2SiO_3 conversion due to CO_2 capture was determined by thermogravimetry; then, the reaction extent of Li_2SiO_3 -carbonation ($X_{\text{Li}_2\text{SiO}_3}$) was defined as follows:

$$X_{\text{Li}_2\text{SiO}_3} = 1 - \frac{n_{\text{Li}_2\text{SiO}_3}(t=t)}{n_{\text{Li}_2\text{SiO}_3}(t=0)}, \quad (4)$$

where $n_{\text{Li}_2\text{SiO}_3}(t=0)$ and $n_{\text{Li}_2\text{SiO}_3}(t=t)$ are the Li_2SiO_3 molar contents of the sample at time $t=0$ and time t , respectively.

As discussed in Sections 3.2 and 3.3, despite the presence of humidity in the CO_2 absorption tests, neither reaction with water nor condensation of physisorbed water are related to the observed final mass gain. Actually, the results suggest that only the carbonation of Li_2SiO_3 is occurring according to reaction (b); hence, the proposed kinetic model is correctly applied. The experimental data of the Li_2SiO_3 carbonation obtained by the thermogravimetric analysis were fitted to Eq. (1). The regression was accomplished using the nonlinear curve fitting function of Origin 8.0 software.

Fig. 10 shows the extent of Li_2SiO_3 carbonation as a function of the reaction time. Isotherms were obtained at different temperatures ranging from of $30\text{--}70^\circ\text{C}$ (Fig. 8(a)–(c)) and constant values of relative humidity RHs ranging from (20 to 80 RH%). Based on the final conversion values, it is clear that carbonation is promoted by both temperature and RH. The highest conversion of Li_2SiO_3 due to CO_2 capture was observed at 50°C and 80% RH and at 70°C and 80% RH. Fig. 10 compares the experimental data (points) and the modeled curves (solid curves). As is shown, the model fitted the experimental data reasonably well. The obtained R^2 coefficients (between 0.984 and 0.998) and the K_1 and K_2 regressed values are listed in Table 3. Through analysis of the obtained kinetic parameters (Table 3), it is clear that K_1 increased and K_2 decreased with increasing temperature and RH. Nevertheless, because the reciprocal of K_2 is directly proportional to the conversion (see Eq. (1)), the observed behavior suggests that carbonation is sensitive to both temperature and humidity.

Finally, it is important to mention that because a thorough kinetic analysis requires to include possible mass transport mechanisms that would take place once a product layer is formed (diffusion controlled regime), Shih's model was satisfactorily used as a first approach to evaluate the effect of both temperature and RH on the carbonation of Li_2SiO_3 powders.

Conclusions

Lithium metasilicate powders were successfully synthesized via a microwave-assisted hydrothermal method to study the effects of several variables, such as reaction time, stirring, and the addition of a surfactant. The proposed synthesis route offers

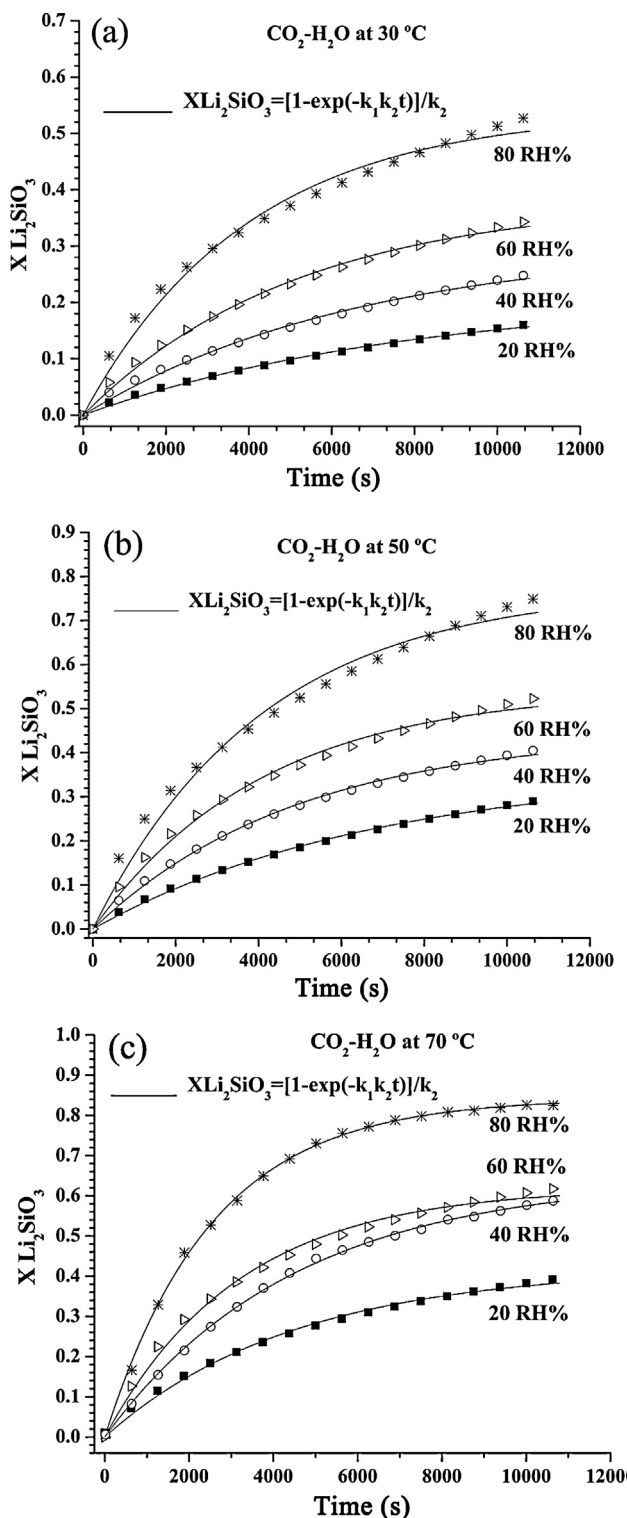


Fig. 10. Kinetic isotherms performed at different temperatures and relative humidities (RHs): (a) 30 °C, (b) 50 °C, and (c) 70 °C. Curves show both the experimental (points) and the modeled data (fitted lines).

the advantages of low temperature (125 °C) and a very short reaction time (15 min) to obtain the pure crystalline phase of Li_2SiO_3 .

The sample characterization revealed the formation of nanocrystalline and porous powders, which exhibited high surface areas. Li_2SiO_3 powders did not show significant reactivity under the high RHs and low temperatures range studied. However, it

Table 3
 CO_2 chemisorption kinetic parameters obtained by applying Shih's model (Shih et al., 1999).

Temperature (°C)	K_1 (s^{-1})	K_2	R^2
20 RH%	3×10^{-5}	4.72	0.995
	5×10^{-5}	2.77	0.998
	9×10^{-5}	2.37	0.995
40 RH%	5×10^{-5}	3.29	0.993
	9×10^{-5}	2.24	0.997
	1.9×10^{-3}	1.68	0.995
60 RH%	7×10^{-5}	2.61	0.995
	1.4×10^{-4}	1.55	0.998
	1.9×10^{-4}	1.29	0.984
80 RH%	1.4×10^{-4}	1.85	0.987
	1.3×10^{-4}	1.83	0.992
	3.3×10^{-4}	1.18	0.998

was observed that Li_2SiO_3 is able to trap CO_2 at low temperatures. In fact, the sorbents showed excellent reactivity in the presence of CO_2 -water vapor mixtures at temperatures ranging from 30 to 70 °C and 20% to 80% RH. The results suggest that both the textual properties of the prepared materials and the presence of water vapor enhanced CO_2 absorption at low temperatures. In addition, the kinetic analysis confirms the importance of temperature and RH during CO_2 -water vapor chemisorption.

Based on previous reports by other authors and the properties observed in the present study, the synthesized materials have potential applications as catalysts and materials for CO_2 capture, among others.

Acknowledgments

This work was supported by the SIP-IPN 2014689 Project. J. Ortiz-Landeros wishes to express his appreciation for the PICPAE-IPN, SIBE-IPN, and EDI-IPN programs.

References

- Alemi, A., Khademinia, S., Joo, S. W., Dolatyari, M., & Bakhtiari, A. (2013). Lithium metasilicate and lithium disilicate nanomaterials: Optical properties and density functional theory calculations. *International Nano Letters*, 3(1), 1–11.
- Bale, C. W., Chartrand, P., Degterov, S. A., Eriksson, G., Hack, K., Mahfoud, R. B., et al. (2002). FactSage thermochemical software and databases. *Calphad*, 26(2), 189–228.
- Carella, E., & Hernández, T. (2012). Ceramics for fusion reactors: The role of the lithium orthosilicate as breeder. *Physica B: Condensed Matter*, 407, 4431–4435.
- Chen, K. T., Wang, J. X., Dai, Y. M., Wang, P. H., Liou, C. Y., Nien, C. W., et al. (2013). Rice husk ash as a catalyst precursor for biodiesel production. *Journal of the Taiwan Institute of Chemical Engineers*, 44, 622–629.
- Cruz, D., & Bulbulian, S. (2003). Synthesis of lithium silicate tritium breeder powders by a modified combustion method. *Journal of Nuclear Materials*, 312, 262–265.
- Cruz, D., Bulbulian, S., Lima, E., & Pfeiffer, H. (2006). Kinetic analysis of the thermal stability of lithium silicates (Li_4SiO_4 and Li_2SiO_3). *Journal of Solid State Chemistry*, 179(3), 909–916.
- Inaguma, Y., & Nakashima, M. (2013). A rechargeable lithium-air battery using a lithium ion-conducting lanthanum lithium titanate ceramics as an electrolyte separator. *Journal of Power Sources*, 228, 250–255.
- Khomane, R. B., Sharma, B. K., Saha, S., & Kulkarni, B. D. (2006). Reverse microemulsion mediated sol-gel synthesis of lithium silicate nanoparticles under ambient conditions: Scope for CO_2 sequestration. *Chemical Engineering Science*, 61, 3415–3418.
- Knitter, R., Chaudhuri, P., Feng, Y. J., Hoshino, T., & Yu, I. K. (2013). Recent developments of solid breeder fabrication. *Journal of Nuclear Materials*, 442, S420–S424.
- Knitter, R., Kolb, M. H., Kaufmann, U., & Goraiab, A. A. (2013). Fabrication of modified lithium orthosilicate pebbles by addition of titania. *Journal of Nuclear Materials*, 442, S433–S436.
- Komarneni, S., & Katsuki, H. (2010). Microwave-hydrothermal synthesis of barium titanate under stirring condition. *Ceramics International*, 36(3), 1165–1169.
- Leofanti, G., Padovan, M., Tozzola, G., & Venturelli, B. (1998). Surface area and pore texture of catalysts. *Catalysis Today*, 41, 207–219.

- Li, X. Q., Guo, H. J., Li, L. M., Li, X. H., Wang, Z. X., Hui, O. U., et al. (2011). Effects of calcination temperature on properties of Li_2SiO_3 for precursor of $\text{Li}_2\text{FeSiO}_4$. *Transactions of Nonferrous Metals Society of China*, 21, 529–534.
- Li, X., & Yang, H. (2014). Morphology-controllable Li_2SiO_3 nanostructures. *CrystEngComm*, 16, 4501–4506.
- Mondragón-Gutiérrez, G., Cruz, D., Pfeiffer, H., & Bulbulian, S. (2008). Low temperature synthesis of Li_2SiO_3 : Effect on its morphological and textural properties. *Research Letters in Material Science*, 2008 <http://dx.doi.org/10.1155/2008/908654>. Article ID 908654, 4 pages
- Nair, B. N., Burwood, R. P., Goh, V. J., Nakagawa, K., & Yamaguchi, T. (2009). Lithium based ceramic materials and membranes for high temperature CO_2 separation. *Progress in Materials Science*, 54, 511–541.
- Nikulshina, V., & Steinfeld, A. (2009). CO_2 capture from air via CaO-carbonation using a solar-driven fluidized bed reactor: Effect of temperature and water vapor concentration. *Chemical Engineering Journal*, 155, 67–873.
- Nikulshina, V., Gálvez, M. E., & Steinfeld, A. (2007). Kinetic analysis of the carbonation reactions for the capture of CO_2 from air via the $\text{Ca}(\text{OH})_2$ – CaCO_3 – CaO solar thermochemical cycle. *Chemical Engineering Journal*, 129, 75–83.
- Nomura, M., Sakanishi, T., Utsumi, Y. N. K., & Nakamura, R. (2013). Preparation of CO_2 permselective Li_4SiO_4 membranes by using mesoporous silica as a silica source. *Energy Procedia*, 37, 1004–1011.
- Ortiz-Landeros, J., Martínez-dlCruz, L., Gómez-Yáñez, C., & Pfeiffer, H. (2011). Towards understanding the thermoanalysis of water sorption on lithium orthosilicate (Li_4SiO_4). *Thermochimica Acta*, 515, 73–78.
- Ortiz-Landeros, J., Contreras-García, M. E., Gómez-Yáñez, C., & Pfeiffer, H. (2011). Surfactant-assisted hydrothermal crystallization of nanostructured lithium metasilicate (Li_2SiO_3) hollow spheres: (I) Synthesis, structural and microstructural characterization. *Journal of Solid State Chemistry*, 184(5), 1304–1311.
- Ortiz-Landeros, J., Gómez-Yáñez, C., & Pfeiffer, H. (2011). Surfactant-assisted hydrothermal crystallization of nanostructured lithium metasilicate (Li_2SiO_3) hollow spheres: II—Textural analysis and CO_2 – H_2O sorption evaluation. *Journal of Solid State Chemistry*, 184, 2257–2262.
- Ortiz-Landeros, J., Gómez-Yáñez, C., López-Juárez, R., Dávalos-Velasco, I., & Pfeiffer, H. (2012). Synthesis of advanced ceramics by hydrothermal crystallization and modified related methods. *Journal of Advanced Ceramics*, 1(3), 204–220.
- Ortiz-Landeros, J., Romero-Ibarra, I. C., Gómez-Yáñez, C., Lima, E., & Pfeiffer, H. (2013). $\text{Li}_{4-x}(\text{Si}_{1-x}\text{Al}_x)\text{O}_4$ solid solution mechanosynthesis and kinetic analysis of the CO_2 chemisorption process. *The Journal of Physical Chemistry C*, 117, 6303–6311.
- Peng, Z. D., Cao, Y. B., Hu, G. R., Du, K., Gao, X. G., & Xiao, Z. W. (2009). Microwave synthesis of $\text{Li}_2\text{FeSiO}_4$ cathode materials for lithium-ion batteries. *Chinese Chemical Letters*, 20, 1000–1004.
- Prasad, A., & Basu, A. (2012). Structural and dielectric studies of Li_2SiO_3 ceramic. *Materials Letters*, 66, 1–3.
- Puna, J. F., Gomes, J. F., Bordado, J. C., Correia, M. J. N., & Dias, A. P. S. (2014). Biodiesel production over lithium modified lime catalysts: Activity and deactivation. *Applied Catalysis A: General*, 470, 451–457.
- Roisnel, T., & Rodriguez-Carvajal, J. (2000). WinPLOTR: A Windows tool for powder diffraction patterns analysis. In *Materials science forum, proceedings of the seventh European powder diffraction conference* (pp. 118–123) (1), 378.
- Romero-Ibarra, I. C., Ortiz-Landeros, J., & Pfeiffer, H. (2013). Microstructural and CO_2 chemisorption analyses of Li_4SiO_4 : Effect of surface modification by the ball milling process. *Thermochimica Acta*, 567, 118–124.
- Rouquerol, J., Rouquerol, F., & Sing, K. (1999). *Adsorption by powders and porous solids: Principles, methodology and applications*. London: Academic Press.
- Shih, S. M., Ho, C. U. S., Song, Y. S., & Lin, J. P. (1999). Kinetics of the reaction of $\text{Ca}(\text{OH})_2$ with CO_2 at low temperature. *Industrial & Engineering Chemistry Research*, 38, 1316–1322.
- Siauciunas, R., Rupsyté, E., Kitrys, S., & Galeckas, V. (2004). Influence of tobermorite texture and specific surface area on CO_2 chemisorption. *Colloids and Surface A: Physicochemical and Engineering Aspects*, 244, 197–204.
- Slagle, O. D., Hollenberg, G. W., & Baldwin, D. L. (1991). The FUBR-1B irradiation experiment: Tritium release and physical stability of solid breeder materials. *Journal of Nuclear Materials*, 179–183, 843–846.
- Somiya, S., & Roy, R. (2000). Hydrothermal synthesis of fine oxide powders. *Bulletin of Materials Science*, 23(6), 453–460.
- Swedlund, P. J., Miskelly, G. M., & McQuillan, A. J. (2009). An attenuated total reflectance IR study of silicic acid adsorbed onto a ferric oxyhydroxide surface. *Geochimica et Cosmochimica Acta*, 73, 4199–4214.
- Tang, T., Zhang, Z., Meng, J. B., & Luo, D. L. (2009). Synthesis and characterization of lithium silicate powders. *Fusion Engineering and Design*, 84, 2124–2130.
- Tatsumisago, M., Takano, R., Tadanaga, K., & Hayashi, A. (2014). Preparation of $\text{Li}_3\text{BO}_3\text{-Li}_2\text{SO}_4$ glass–ceramic electrolytes for all-oxide lithium batteries. *Journal of Power Sources*, 270, 603–607.
- Wang, J. X., Chen, K. T., Huang, S. T., & Chen, C. C. (2011). Application of Li_2SiO_3 as a heterogeneous catalyst in the production of biodiesel from soybean oil. *Chinese Chemical Letters*, 22, 1363–1366.
- Wang, J. X., Chen, K. T., Wu, J. S., Wang, P. H., Huang, S. T., & Chen, C. C. (2012). Production of biodiesel through transesterification of soybean oil using lithium orthosilicate solid catalyst. *Fuel Processing Technology*, 104, 167–173.
- Wang, J., Huang, L., Yang, R., Zhang, Z., Wu, J., Gao, Y., et al. (2014). Recent advances in solid sorbents for CO_2 capture and new development trends. *Energy & Environmental Science*, 7(11), 3478–3518.
- Yang, A., Wang, H., Li, W., & Shi, J. (2012). Synthesis of lithium metasilicate powders at low temperature via mechanical milling. *Journal of the American Ceramic Society*, 95(6), 1818–1821.
- Yang, W. C. (2010). Particuology and climate change. *Particuology*, 8(6), 507–513.
- Zhang, B., Nieuwoudt, M., & Easteal, A. J. (2008). Sol–gel route to nanocrystalline lithium metasilicate particles. *Journal of the American Ceramic Society*, 91(6), 1927–1932.